palgrave communications
HUMANITIES | SOCIAL SCIENCES | BUSINESS

ARTICLE

https://doi.org/10.1057/s41599-020-0454-z OPEN

When was silcrete heat treatment invented in South Africa?

Patrick Schmidt [1,2]✉, Deano Stynder[3], Nicholas J. Conard[1] & John E. Parkington[3]

ABSTRACT Silcrete heat treatment, along with a suit of other innovations, have been used to argue for an early onset of modern or complex behaviours in Middle Stone Age hominins. This practice was confined to South Africa's southern and western Cape regions where it was continuously practised since the Still Bay industry. However, the exact moment that this technological advancement occurred still remains unclear. This is partly due to the scarcity of silcrete assemblages dating to the first half of the Middle Stone Age. To determine when silcrete heat treatment began to be well-established, we compare the silcrete assemblages from two archaeological sites situated along the south western coast of South Africa: Hoedjiespunt 1, one of the earliest Middle Stone Age silcrete assemblages dating to 119–130 ka, and Duinefontein 2, one of the latest Early Stone Age assemblages dating to 200–400 ka. Our results suggest that the invention of heat treatment occurred sometime between 130 ka and 200–400 ka, as it is still absent in the earlier assemblage but fully mastered and well-integrated in the recent one. This period corresponds to the time that *Homo sapiens* became the major hominin species in the southern African subcontinent and it is roughly the time that silcrete use became widespread in the second half of the Cape-coastal Middle Stone Age. This opens interesting new questions on the relation between silcrete use and heat treatment and on why early modern humans spontaneously invented heat treatment when they began using silcrete in the Cape region.

[1] Eberhard Karls University of Tübingen, Department of Early Prehistory and Quaternary Ecology, Schloss Hohentübingen, 72070 Tübingen, Germany.
[2] TRACES – UMR 5608 Université Toulouse - Jean Jaurès, Maison de la Recherche, 5 allée Antonio Machado, 31058 TOULOUSE Cedex 9, France.
[3] University of Cape Town, Department of Archaeology, Rondebosch, 7701, South Africa. ✉email: patrick.schmidt@uni-tuebingen.de

Introduction

Silcrete heat treatment is commonly understood as a technical process that aims at improving the quality of raw materials for knapping. It has in the past decade become one of the arguments for an early onset of modern or complex behaviours in the Middle Stone Age (MSA) (see for example: Sealy, 2009; Wadley, 2013). This is because it was argued to proxy for several archaeological and anthropological traits like abstract thinking (Wadley and Prinsloo, 2014) or high investments in resources (Brown and Marean, 2010). Although other authors (Schmidt et al., 2015; Schmidt et al., 2013) have argued against such interpretations, the early appearance of heat treatment unquestionably documents one the first moments humans attempted to transform their material world with fire (Stolarczyk and Schmidt, 2018). Knowing the exact moment of its first invention is therefore a crucial factor for our understanding of human evolution.

When heat treatment was first documented at Pinnacle Point (Brown et al., 2009), the main argument was made for the Howiesons Poort (HP; roughly dated to 50–85 ka, depending on what site it was found at). The same paper, also proposed that heat treatment may have been invented as early as 164 ka. This is even more interesting, as this date falls into a period where silcrete use was generally rare in southern Africa (Will and Mackay, 2017). In fact, except at Pinnacle Point, there are no other assemblages in the Cape from before ~130 ka that yielded more than a handful of silcrete pieces, and there is no silcrete outside of the Cape coastal zone at all. This situation is uncomfortable for MSA archaeologists. All MSA silcrete assemblages younger than the Stillbay (SB; ~70–80 ka) that were inspected for heat treatment have yielded abundant heated artefacts (see for example: Schmidt and Högberg, 2018; Delagnes et al., 2016; Schmidt et al., 2015). With few exceptions (for one exception see: Schmidt and Mackay, 2016), the relative prevalence of heat treatment varies between ~70 and >90% in these silcrete assemblages. Thus, at least from the SB onwards, heat treatment seems to have been an important step in the reduction sequences associated with silcrete. The possibility to artificially improve its knapping quality might even have governed the choice of using silcrete as a raw material. At least, there seems to be a correlation between silcrete use and heat treatment that needs to be explained. There are, however, two arguments that might change our view on MSA heat treatment. It has been argued that heat treatment might not have been practised to improve knapping quality but rather for heat-fracturing raw material blocks, to reduce nodule size before knapping even began (Schmidt et al., 2015; Porraz et al., 2016). This argument was proposed because at some sites, many silcrete blocks broke from the action of fire before knapping (see for example: Schmidt et al., 2015; Delagnes et al., 2016). Improved knapping quality would in this case only be a by-product. The other argument is that natural fires might have caused what archaeologists recognise as heat treatment. It could be imagined that bushfires or fire-based site maintenance (Goldberg et al., 2009) produced accidentally heated silcrete. If this were the case, the entire MSA heat treatment signal might not reflect any human activity at all.

Based on these considerations a few important questions can be posed: do all silcrete assemblages in the Cape coastal region show signs of heat treatment? If heating proxies, as they have been used to identify heat treatment in MSA assemblages so far, can be identified on all silcrete assemblages regardless of their age, it might be worthwhile to investigate the bushfire hypothesis or other natural causes. If on the other hand, we can identify silcrete assemblages without heat treatment, the bushfire hypothesis becomes unlikely. In the latter case, if intentional heat treatment were real, the time of its invention becomes important. For example, can we identify a gradual onset of heat treatment during the MSA or did it appear with the earliest silcrete use in the MSA? Was there a period in the MSA where unheated silcrete was used? If there was, can we determine at least approximately when heat treatment was invented? If there was not, we may conclude that at least in early assemblages there was an intricate, perhaps causal, relationship between silcrete use and heat treatment.

One way to approach these questions is by investigating the earliest silcrete-bearing MSA assemblages and comparing them with silcrete assemblages from before the MSA. Some of the oldest known silcrete assemblages that have yielded sufficient artefacts for such a study come from sites located on the south western coast of South Africa (Will and Mackay, 2017). There, two sites from between 100 and 130 ka are potential candidates for our study: Ysterfontein 1, initially dated to between 120 and 132 ka (Avery et al., 2009) and Hoedjiespunt 1 (HDP1) initially dated to between 100 and 130 ka (Will et al., 2013). As the Ysterfontein 1 assemblage appears problematic (the dates were rejected, see: Avery et al., 2009) and the HDP assemblage can confidently be attributed to MIS 5e (119–130 ka), we chose the latter. The Western Cape region also provides a large enough silcrete assemblages from before, but still reasonably close to, the MSA: The assemblage from Duinefontein 2 (DFT2), dating to 200–400 ka, is one of these. We included DFT2 in our study investigating whether heating proxies are associated with all coastal silcrete assemblages (i.e., also in the Early Stone Age) or whether heat treatment was confined to the MSA.

Methods

Samples and sample preparation. We inspected 200 silcrete artefacts >5 mm recovered in situ from (DFT2) for macroscopic indicators of heat treatment. These artefacts were randomly chosen by picking bags, one after the other, each time inspecting all silcrete artefacts from within the bags. No other selection (size except for >5 mm, weight, typology) was made prior to inspecting the artefacts for indicators of heat treatment. The site's aeolian sands were estimated to date between 400 and 200 ka based on its faunal record (Klein et al., 1999). We chose DFT2 here because of its geographical proximity to HDP (~85 km), because of the relative abundance of silcrete artefacts and because it has been mentioned as one of the latest Acheulian site in the Western Cape region (Patterson et al., 2016). It is therefore suitable as a pre-MSA point in this study. Seventy-two of these silcrete pieces underwent a quantitative surface roughness analysis using the replica tape method (Schmidt, 2019). In parallel, we inspected 121 artefacts from HDP for macroscopic indicators of heat treatment. Forty-one of these came from the HDP1 site (Will et al., 2013) and the remaining 79 came from HDP3 (Parkington, 2003). The HDP1 deposit was attributed to MIS 5e (119–130 ka) based on radiometric dates and sea level correlation (Will et al., 2013) and, although no radiometric dates have been obtained from HDP3, it nevertheless seems likely, from a point of view of stratigraphy, that artefacts from both sites are of the same age (Parkington, 2003). There is currently a research project attempting to obtain an absolute age for the HDP3 deposit. While results have not been published yet, one of their observations relevant to our study is that the HDP3 sediments were likely deposited during the last interglacial, as revealed by paleoclimatic arguments (Hare, 2020, pers. comm.). Contemporaneity of HDP1 and 3 is, therefore, highly likely, based on stratigraphy and paleoclimate. Fifty-two of these silcrete artefacts from HDP underwent quantitative surface roughness analysis using the replica tape method. We chose not to integrate artefacts made from one silcrete type in our analysis. There is a coarse-grained silcrete with a clast size ranging up to

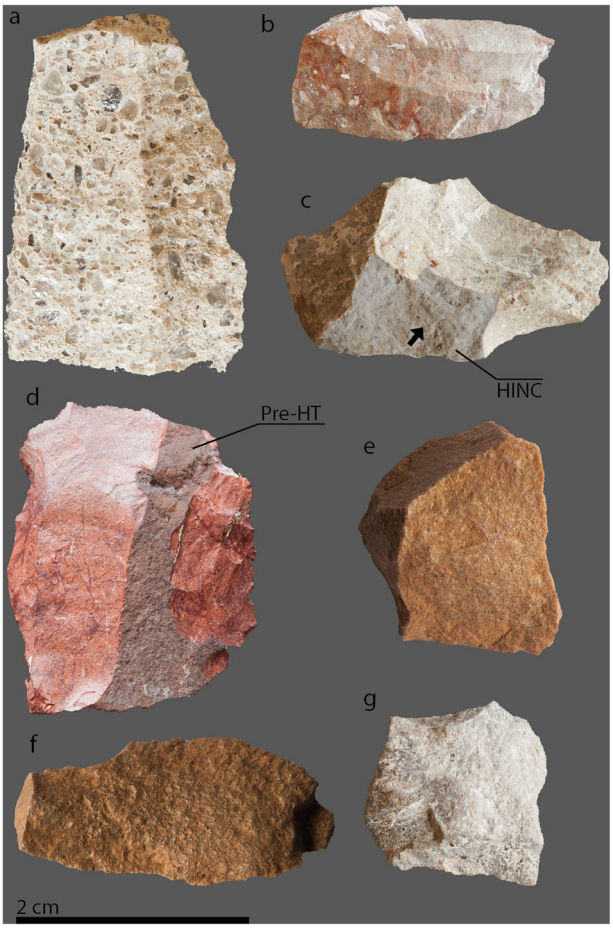

Fig. 1 Photos of analysed Lithic pieces from Hoedjiespunt (**a**–**d** and **g**) and Duinefontein 2 (**e** and **f**). **a** coarse-grained silcrete from Hoedjiespunt excluded from this study. **b** Heat-treated artefact entirely covered by smooth post-heating scars. **c** Heat-treated artefact with a heat-induced non-conchoidal (HINC) fracture surface (artificially darkened for better recognition in this photo). Note the scalar features indicted by the black arrow. **d** Heat-treated artefact with a remnant rougher pre-heating scar (artificially darkened for better recognition in this photo) that is cross-cut by smoother post-heating scars. **e**–**g** Unheated artefacts entirely covered by rough pre-heating scars.

>2 mm in the HDP assemblage (Fig. 1a). It can be difficult to distinguish heat-treated from unheated silcrete with similarly large clasts, based on fracture pattern (Schmidt et al., 2019). In total, there were 20 artefacts of this silcrete type in the HDP assemblage that we excluded from our analysis.

In parallel, an experimental references collection was produced from 30 South African west coast silcrete types. Geological samples were collected in a large area between the town of Hopefield and the Olifants river, an area measuring ~160 km north-south. Samples were chosen to represent a large variety in terms of grain-size and texture. To produce the reference collection, a control flake was removed from each sample, the remaining samples were heat-treated at 450 °C (heating ramp of 4 h, hold time at maximum temperature 2 h; for justification of these parameters see: Schmidt et al., 2017; Schmidt et al., 2016b) and a second flake was removed after the samples had cooled to room temperature. The roughness data measured on this 60-piece references collection is published in tabular form elsewhere (Schmidt, 2019, Table 2) but they are used here as comparison with our DFT2 and HDP archaeological data.

Visual classification of heating proxies. As initially proposed by Schmidt et al. (2015) and subsequently applied during several other studies on heat treatment in the South African MSA and LSA (Delagnes et al., 2016; Porraz et al., 2016; Schmidt and Mackay, 2016), four proxies were used for this visual classification: [1] *Pre-heating removal scars*: relatively rough fracture surfaces corresponding to the removal of flakes from unheated silcrete (Fig. 1e–g). [2] *Post-heating removal scars*: relatively smooth fracture surfaces that correspond to the removal of flakes from heat-treated silcrete (Fig. 1b). [3] *Heat-induced non-conchoidal (HINC) fractures*: surfaces produced by thermal fracturing in a fire (sometimes termed overheating (Schmidt, 2014)). HINC fracture surfaces can be recognised due to their strong surface roughness, the presence of scalar features on the surface (Schmidt et al., 2015) and concave morphologies with frequent angular features (Fig. 1c). Fracture surfaces were only identified as HINC fractures when they are cross-cut by a post-heating removal. This technological relationship indicates that the failure occurred during heat treatment, i.e., within the lithic reduction sequence, and that the reduction was continued afterwards. In the opposite case, when such a fracture surface is not cross-cut by a flake removal, it may result from fracturing at any stage, e.g., during accidental burning after discard, so that no technological information concerning heat treatment can be retrieved from it. [4] *Tempering residue*: a black organic tar (wood tar) produced by dry distillation of plant exudations that was deposited on the silcrete surface during its contact with glowing embers during burning (Schmidt et al., 2016a; Schmidt et al., 2015).

In some previous work (Delagnes et al., 2016; Schmidt et al., 2015) these heating proxies were identified on artefacts through a piece-by-piece comparison with an experimental (external) reference collection. Here, the assignment to different heating proxy categories was solely based on an "internal calibration" (Schmidt, 2019): first, artefacts made from different silcrete types, that show a clearly distinguishable roughness contrast between adjacent pre- and post-heating removal scars on their dorsal side (Fig. 1d), were selected. Such pieces are called 'diagnostic' artefacts because the roughness difference between two adjacent scars on one side of a single piece (provided that the smooth scar is posterior to the rough scar) cannot be explained by different silcrete types, inner sample heterogeneity or taphonomy, i.e., only one explanation of this pattern is left: rough pre- and smoother post-heating removal scars result from knapping before and after heat treatment, respectively, (Schmidt et al., 2019), meaning that these pieces document a stage of pre-heating knapping, the transformation of their fracture mechanics (heat treatment) and a second stage of post-heating knapping. Such pieces have consistently been used to identify heat treatment in assemblages since the beginning of archaeological research on heat treatment (see for example: Bordes, 1969; Inizan et al., 1976; Inizan and Tixier, 2001; Binder, 1984; Binder and Gassin, 1988; Léa, 2004; Léa, 2005; Terradas and Gibaja, 2001; Mandeville, 1973; Marchand, 2001; Mourre et al., 2010; Tiffagom, 1998; Wilke et al., 1991). In light of these considerations and the acceptance of diagnostic pieces in the archaeological community, it can be concluded that they unambiguously result from heat treatment and, consequently, that they can be used as comparative reference to identify pre- and post-heating fracture scars on undiagnostic samples (provided that these are made from the same silcrete types). The known pre- and post-heating scars on diagnostic artefacts were therefore used to 'calibrate' the identification of pre- and post-heating scars on the other undiagnostic artefacts made from the respective silcrete types. Practically, this meant that a set of diagnostic artefacts was laid out on a large table and all other undiagnostic artefacts were compared with the pre- and post-heating scars on these diagnostic pieces. Artefacts that could

not be clearly identified as belonging to one of the frequently occurring silcrete types (for which no diagnostic comparisons could be identified) were left indeterminate in this study. HINC surfaces were identified through the presence of concave, sometimes angular, structures and scalar features (Schmidt et al., 2015).

Surface roughness measurements with replica tape. To estimate the quality of this visual classification of heat treatment proxies, quantitative fracture surface analysis was conducted using replica tape for three-dimensional (3D) surface mapping. The replica tape method is explained in detail in Schmidt (2019) and only the details absolutely necessary are repeated here. A layer of compressible foam is applied with force to the measured surface (the method it is entirely non-destructive). The foam replicates the surface irreversibly by creating a negative of it. The so-produced surface negative contains thicker and thinner parts that correspond to the valleys and peaks of the original surface, respectively. These thicker and thinner areas on the replica tape, when scanned by light transmission, appear more or less transparent. Transparency values measured in this way can then be converted to a 3D map of the surface. To perform these scans, a DeFelsko PosiTector RTR-P tape reader was used in combination with optical grade Testex PRESS-O-FILM replica tape of the grades Coarse and X-Coarse. Measurements made on DFT2 artefacts (ventral surface was measured where possible) were compared with roughness data of the west coast reference collection (as in: Schmidt, 2019, Table 2). For the HDP assemblage, an "internal reference" of surface roughness measurements was established: measurements on diagnostic artefacts, i.e., artefacts with both pre- and post-heating scars, were used as reference measurements. Ten pre-heating removal scars, large enough for replica tape measurements, and 13 suitable post-heating removal scars were identified on HDP diagnostic artefacts. The advantage of such an internal calibration is that, instead of using our external reference collection containing a random number of silcrete types from the greater west coast region, with this method only the silcrete types actually used at HDP are taken into account. The 3.8×3.8 mm wide 3D surface models resulting from replica tape measurements were processed using the Gwyddion free software package. Two statistical quantities were extracted from the 3D surface maps (no filtering applied): the mean roughness (Ra) in µm and the dimensionless differential entropy S of the height value distribution (or Shannon differential entropy, Shannon, 1948). As proposed by Schmidt (2019), we transformed Ra values to their natural logarithm, so that the data can be fitted with a linear function in a scatter plot of S over Ln(Ra). As both values are tightly correlated, the variance between samples in such a plot is one-dimensional and lies on the fitted function (the best fit of the scatter plot). Data quality can be visually estimated by evaluating the straying of data plots around the fitted function. It can be quantified by calculating the mean distance of the plots from this function.

Results

Visual inspection. The fracture patterns on DFT2 silcrete artefacts are rather rough looking. Only one of the four criteria described in section 'Visual classification of heating proxies' can be observed: rough pre-heating removal surfaces. None of the artefacts showed recognisable roughness contrast between adjacent fracture negatives or between different artefacts.

On the other hand, three of the four proxies described in section 'Visual classification of heating proxies' can be observed on HDP artefacts. Although silcrete types from both sites are fairly similar macroscopically, only surfaces on the HDP assemblage could be assigned to distinct groups using the visual identification protocol. These groups are summarised in Table 1. Most artefacts were knapped after heat treatment. Depending on whether undetermined artefacts are included or not, 65–73% of all pieces show traces of heat treatment (smooth post-heating surfaces). On 30% of these heated artefacts, remnants of rough pre-heating surfaces are preserved along, and cross-cut by, a second generation of smoother post-heating scars (these are the diagnostic artefacts). Nine percent of the heat-treated artefacts show signs of heat-induced fracturing during heat treatment (HINC fractures) after which knapping continued. None of the artefacts show black tempering residue.

Surface roughness measurements. Figure 2a is a plot of Ln(Ra) and S values measured on unheated and experimentally heated reference samples from the West Coast region (as taken from: Schmidt, 2019). Figure 2b is a plot of our DFT2 data onto the fitted function of the reference data ($S = 0.826\mathrm{Ln(Ra)} - 11.86$). Values measured on artefacts are summarised in Table 2. The reference scatter plot (Fig. 2a) can be separated into three areas: a zone where only heat-treated samples plot in the lower left corner; a zone where both heated and unheated samples plot in the middle (the indeterminate zone); and a zone in the top right corner where only unheated samples plot. Only the zone in the lower left of the plot, where no unheated reference samples plot, is of importance here. Its limit is marked by a black line perpendicular to the data plots' best fit. Comparing Fig. 2a, b, it can be seen that none of the DFT2 artefacts plot into the heat-treated reference zone to the lower left of this black line. The results for all DFT2 samples are therefore listed as either Indet. or Not-heated in Table 2. In other words, all surfaces on DFT2 artefacts yielded roughness values that can be comfortably explained by unheated west coast silcretes. None of the DFT2 artefacts would have yielded roughness values only explicable by heat-treated

Table 1 Results of the heating proxy analysis of silcrete from Hoedjiespunt.

Silcrete from HDP, total of analysed artefacts: 121	Count	Percent total	Percent det.	Percent HT
Indeterminate artefacts	12	9.9%		
Not-heated artefacts	30	24.8%	27.5%	
Artefacts with post-heating removal scars	79	65.3%	72.5%	
Of which:				
Diagnostic artefacts (pre- and post-HT scars)	24			30.4%
Artefacts with HINC-fracture surfaces	7			8.9%
Artefacts with black tempering residue	0			0%

Percentages under 'Percent total' refer to the total of analysed artefacts, percentages under 'Percent det.' refer to all determinable artefacts in the assemblage but exclude indeterminate artefacts. Percentages under 'Percent HT' refer to the number of heat-treated artefacts in the assemblage. Percentages in the section 'of which:' are calculated to the base of all artefacts with post-heating removal scars (79). Note that percentages below 'of which:' are not exclusive, i.e., there are diagnostic artefacts that also contain HINC fractures or tempering residue.

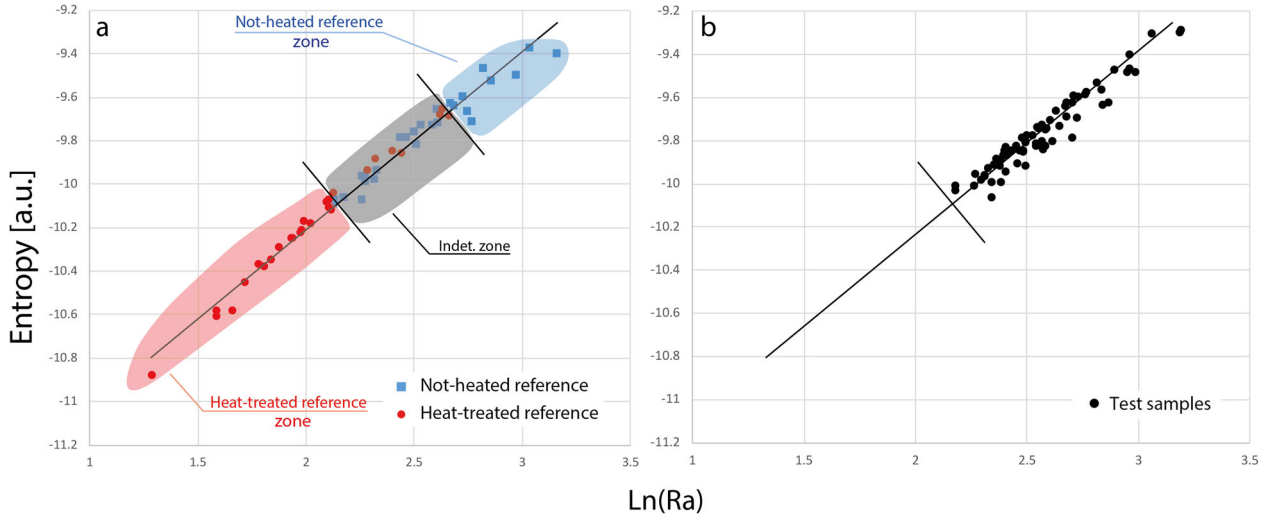

Fig. 2 Plots of the entropy S and mean roughness Ra values of archaeological samples from Duinefontein 2. a Plot of 60 experimental reference samples (30 not-heated+30 heated) from the South African Western Cape region and their linear best fit (data from Schmidt, 2019). The black line marks the threshold, left of which no unheated samples plot, i.e., all unheated reference samples plot to the upper right of the line. The line cuts the best fit at Ln(Ra): 2.12. **b** Plot of 72 archaeological test samples onto the same fitted function and threshold line. Note that none of Duinefontein 2 test samples show values that could not be explained by the variability of unheated Western Cape silcrete.

west coast silcrete. Thus, there is no reason to suggest that any of the DFT2 artefacts were heat-treated.

Figure 3a is a plot of Ln(Ra) and *S* values measured on diagnostic artefacts from HDP onto the fields of the heated-, unheated- and indeterminate zone of west coast reference samples (best fit and zone limits of HDP data in continuous lines; in broken lines for reference data). Comparing both, post-heating surfaces from HDP roughly plot in the same zone as heat-treated reference samples. Most HDP pre-heating surfaces plot in the reference samples' indeterminate zone. This is because the analysed HDP silcrete assemblage is finer-grained than some of the west coast reference silcretes (i.e., yielding overall lower *S* and Ln(Ra) values), so that comparing them is inadvisable. Our estimation of the number of heated artefacts in the HDP test group (undiagnostic artefacts in Fig. 3b) is therefore based on a comparison with known pre- and post-heating surfaces from the same assemblage (internal calibration, Schmidt, 2019). This is shown in Fig. 3b. Black lines perpendicular to the best fit of the data ($S = 0.833\mathrm{Ln(Ra)} - 11.92$) indicate the boundaries of the indeterminate zone, as measured on known pre- and post-heating surfaces (Fig. 3a). Unlike the DFT2 data, this HDP plot can be separated into three zones, indicating that there are heat-treated and unheated samples (one sample is indeterminate). Our HDP surface roughness analysis allows the classification of 34 (65%) pieces as heat-treated and 17 (33%) unheated (Table 2). Thus, the number of heat-treated artefacts is in agreement with the data obtained by visual inspection; the number of unheated artefacts is 8% higher than found during visual inspection.

Discussion

We found no sign of heat treatment in the silcrete assemblage from the late Acheulean site of Duinefontein 2. During visual inspection, we observed neither roughness contrast, nor particularly smooth fracture surfaces. Replica tape surface roughness analysis showed that the fracture patterns on DFT2 flake scars fall in the range of unheated silcrete. The quality of this roughness data is expressed by the mean distance of all test data points from their fitted function (in Euclidean distance in the scatter plot). The mean distance for our DFT2 data is 0.031. This value lies slightly above the values obtained during previous studies (0.022, as recalculated from artefact data in: Schmidt, 2019; and 0.02, as recalculated from the data in: Schmidt and Hiscock, 2019). Thus, the quality of our DFT2 artefact roughness data appears to be 30–35% worse than in previous similar studies. The reasons for this are unclear and a more precise interpretation of mean distance values must await future studies providing more scattering distance data. However, we note that the data points of our experimental west coast reference collection scatter around their fitted function with a mean of 0.028 (as recalculated from reference samples data in: Schmidt, 2019), being in agreement with our DFT2 distance data within 10%. Thus, based on our visual and roughness data there is no reason to suggest that there was heat treatment in the Acheulian of DFT2. This has one important consequence: the visually observable heat treatment signal, smooth post-heating fracture surfaces, is not ubiquitous on archaeological silcretes from the South African silcrete coastal belt. While this might seem insignificant or even common-sense at first glance, we note that our study is the first to specifically investigate this question. Several studies have so far shown the abundance of heat-treated silcrete artefacts in the South African MSA (see among others: Delagnes et al., 2016; Porraz et al., 2016; Schmidt and Mackay, 2016; Schmidt et al., 2015); in fact almost all silcrete-bearing MSA sites have yielded abundant heat-treated artefacts so far. Our description of an unheated older silcrete assemblage sustains the argument that heating proxies (like smooth post-heating fractures) are not an intrinsic property of archaeological silcrete assemblages, but are specific to the MSA in this region and they can be used to identify and quantify heat treatment. The latter of these statements is based on the study of a single pre-MSA site only. This is mainly due to the scarcity of late ESA sites that yielded silcrete assemblages. Based on this samples number ($n = 1$), it cannot be entirely ruled out that the absence of ESA heat treatment in our study may have been caused by other factors like site-use, technology or settlement patterns that were only active at DFT2. We do, however, note that heat treatment has never been suggested elsewhere in the MSA and, given our first observations at DFT2, it appears highly unlikely that there was ESA heat treatment.

We found a different pattern in the MSA at Hodjiespunt (MIS5e, 130–119 ka). There, most of the analysed silcrete artefacts

Table 2 Results of the replica tape measurements of archaeological test samples.

Site	Sample no.	Ra [µm]	Ln(Ra)	*S*	*x* on function [Ln(Ra)]	*y* on function [S]	Result
DFT2	200888	11.75	2.464	−9.85	2.454	−9.83	Indet.
DFT2	200121	13.06	2.570	−9.84	2.519	−9.78	Indet.
DFT2	200143	12.69	2.541	−9.82	2.510	−9.79	Indet.
DFT2	200146	9.60	2.262	−10.01	2.253	−10.00	Indet.
DFT2	200151	18.00	2.890	−9.47	2.892	−9.47	Not-heated
DFT2	200167	13.31	2.589	−9.74	2.579	−9.73	Indet.
DFT2	200172	14.94	2.704	−9.62	2.707	−9.62	Not-heated
DFT2	200199	16.66	2.813	−9.53	2.816	−9.53	Not-heated
DFT2	200200	10.82	2.381	−9.99	2.333	−9.93	Indet.
DFT2	200203	24.20	3.186	−9.30	3.153	−9.26	Not-heated
DFT2	200205	13.63	2.612	−9.80	2.564	−9.74	Indet.
DFT2	200209	15.21	2.722	−9.70	2.681	−9.65	Not-heated
DFT2	200210	8.83	2.178	−10.03	2.193	−10.05	Indet.
DFT2	200250	11.38	2.432	−9.85	2.435	−9.85	Indet.
DFT2	200265	11.89	2.476	−9.79	2.489	−9.80	Indet.
DFT2	200266	12.50	2.526	−9.77	2.526	−9.77	Indet.
DFT2	200268	24.20	3.186	−9.30	3.153	−9.26	Not-heated
DFT2	200298	13.23	2.582	−9.83	2.534	−9.77	Indet.
DFT2	200312	14.89	2.701	−9.78	2.625	−9.69	Indet.
DFT2	200329	10.63	2.364	−9.88	2.376	−9.90	Indet.
DFT2	200330	14.04	2.642	−9.73	2.615	−9.70	Indet.
DFT2	200349	12.97	2.563	−9.82	2.523	−9.78	Indet.
DFT2	200354	12.07	2.491	−9.92	2.435	−9.85	Indet.
DFT2	200376	19.06	2.948	−9.48	2.921	−9.45	Not-heated
DFT2	200423	13.25	2.584	−9.75	2.574	−9.73	Indet.
DFT2	200428	11.24	2.419	−9.85	2.427	−9.86	Indet.
DFT2	200435	10.84	2.383	−9.89	2.385	−9.89	Indet.
DFT2	200440	12.17	2.499	−9.77	2.510	−9.79	Indet.
DFT2	200481	14.55	2.678	−9.69	2.657	−9.67	Not-heated
DFT2	200485	12.11	2.494	−9.81	2.490	−9.80	Indet.
DFT2	200487	10.49	2.350	−9.91	2.355	−9.92	Indet.
DFT2	200490	19.74	2.983	−9.48	2.942	−9.43	Not-heated
DFT2	200507	21.34	3.061	−9.30	3.076	−9.32	Not-heated
DFT2	200522	16.99	2.833	−9.56	2.813	−9.54	Not-heated
DFT2	200534	17.05	2.836	−9.63	2.780	−9.56	Not-heated
DFT2	200541	11.95	2.481	−9.85	2.463	−9.83	Indet.
DFT2	200545	11.67	2.457	−9.91	2.420	−9.86	Indet.
DFT2	200548	10.36	2.338	−9.99	2.307	−9.95	Indet.
DFT2	200568	12.68	2.540	−9.81	2.514	−9.78	Indet.
DFT2	200607	11.98	2.483	−9.85	2.464	−9.83	Indet.
DFT2	200791	14.51	2.675	−9.62	2.689	−9.64	Not-heated
DFT2	200808	15.81	2.761	−9.58	2.759	−9.58	Not-heated
DFT2	200809	12.07	2.491	−9.80	2.492	−9.80	Indet.
DFT2	200817	10.41	2.343	−10.06	2.276	−9.98	Indet.
DFT2	200822	13.04	2.568	−9.73	2.573	−9.73	Indet.
DFT2	200825	10.07	2.310	−9.97	2.302	−9.96	Indet.
DFT2	200852	12.84	2.553	−9.74	2.558	−9.75	Indet.
DFT2	200866	12.75	2.546	−9.74	2.556	−9.75	Indet.
DFT2	200882	15.02	2.709	−9.59	2.724	−9.61	Not-heated
DFT2	200883	13.82	2.626	−9.66	2.640	−9.68	Indet.
DFT2	200889	11.00	2.398	−9.85	2.415	−9.87	Indet.
DFT2	200890	10.94	2.392	−9.87	2.400	−9.88	Indet.
DFT2	200903	19.30	2.960	−9.40	2.967	−9.41	Not-heated
DFT2	200913	24.29	3.190	−9.29	3.160	−9.25	Not-heated
DFT2	200921	11.07	2.404	−9.83	2.425	−9.86	Indet.
DFT2	200922	14.43	2.669	−9.64	2.677	−9.65	Not-heated
DFT2	200923	13.49	2.602	−9.70	2.606	−9.71	Indet.
DFT2	200942	15.30	2.728	−9.59	2.735	−9.60	Not-heated
DFT2	200943	10.77	2.377	−9.92	2.367	−9.90	Indet.
DFT2	200963	10.23	2.325	−9.93	2.330	−9.94	Indet.
DFT2	201042	10.09	2.312	−9.96	2.307	−9.95	Indet.
DFT2	rNo. 1	11.57	2.448	−9.82	2.457	−9.83	Indet.
DFT2	rNo. 2	17.55	2.865	−9.63	2.800	−9.55	Not-heated
DFT2	rNo. 3	11.10	2.407	−9.87	2.408	−9.87	Indet.
DFT2	rNo. 4	9.89	2.292	−9.98	2.284	−9.97	Indet.
DFT2	rNo. 5	15.92	2.768	−9.57	2.769	−9.57	Not-heated

Table 2 (continued)

Site	Sample no.	Ra [μm]	Ln(Ra)	*S*	*x* on function [Ln(Ra)]	*y* on function [S]	Result
DFT2	rNo. 6	19.31	2.961	−9.47	2.935	−9.44	Not-heated
DFT2	rNo. 7	8.83	2.178	−10.01	2.203	−10.04	Indet.
DFT2	rNo. 8	11.19	2.415	−9.85	2.422	−9.86	Indet.
DFT2	rNo. 9	9.63	2.265	−9.95	2.283	−9.97	Indet.
DFT2	rNo. 10	13.02	2.566	−9.80	2.538	−9.76	Indet.
DFT2	rNo. 11	11.08	2.405	−9.94	2.372	−9.90	Indet.
HDP1	L12-3432	9.54	2.255	−9.96	2.295	−10.01	Not-heated
HDP1	K11-0014	7.38	1.999	−10.20	2.026	−10.23	Heated
HDP1	K11-0016	6.61	1.889	−10.33	1.897	−10.34	Heated
HDP1	K12-0234	4.71	1.550	−10.61	1.560	−10.62	Heated
HDP1	K13-0026	6.26	1.834	−10.33	1.865	−10.37	Heated
HDP1	L11-0021	8.80	2.175	−10.05	2.204	−10.08	Not-heated
HDP1	L11-0048	11.52	2.444	−9.79	2.489	−9.85	Not-heated
HDP1	L12-0394	5.25	1.658	−10.53	1.663	−10.54	Heated
HDP1	L12-0828	7.26	1.983	−10.19	2.021	−10.24	Heated
HDP1	M11-0195	6.20	1.825	−10.35	1.849	−10.38	Heated
HDP1	M11-0262	9.05	2.203	−10.05	2.220	−10.07	Not-heated
HDP1	M11-1803	7.12	1.963	−10.25	1.980	−10.27	Heated
HDP1	M11-2204	7.67	2.037	−10.15	2.073	−10.19	Heated
HDP1	M11-2371	8.39	2.127	−10.20	2.102	−10.17	Heated
HDP1	M12-0017	9.88	2.291	−10.14	2.228	−10.06	Not-heated
HDP1	M12-0081	8.35	2.122	−10.11	2.143	−10.14	Indet.
HDP1	M12-0199	9.00	2.197	−10.00	2.242	−10.05	Not-heated
HDP1	M12-0217	5.66	1.734	−10.44	1.751	−10.46	Heated
HDP1	M12-0225	5.22	1.653	−10.58	1.635	−10.56	Heated
HDP1	M12-2203	8.40	2.128	−10.05	2.176	−10.11	Not-heated
HDP1	M12-3121	4.85	1.580	−10.61	1.577	−10.61	Heated
HDP1	M12-3122	7.59	2.027	−10.19	2.048	−10.21	Heated
HDP1	M12-3372	12.48	2.524	−9.74	2.560	−9.79	Not-heated
HDP1	M12-3554	9.33	2.233	−10.01	2.258	−10.04	Not-heated
HDP1	M13-0014	21.09	3.049	−9.38	3.050	−9.38	Not-heated
HDP1	N12-0012	12.48	2.524	−9.74	2.560	−9.79	Not-heated
HDP1	N13-0891	11.72	2.461	−9.82	2.486	−9.85	Not-heated
HDP1	rNo. 1	5.48	1.701	−10.48	1.712	−10.49	Heated
HDP1	rNo. 2	9.00	2.197	−10.11	2.187	−10.10	Not-heated
HDP1	rNo. 3	13.77	2.622	−9.73	2.625	−9.73	Not-heated
HDP1	rNo. 4	6.70	1.902	−10.30	1.920	−10.32	Heated
HDP3	rNo. 5	7.17	1.970	−10.22	1.999	−10.26	Heated
HDP3	rNo. 6	5.20	1.648	−10.51	1.667	−10.53	Heated
HDP3	rNo. 7	10.31	2.333	−9.96	2.339	−9.97	Not-heated
HDP3	rNo. 8	4.12	1.417	−10.73	1.422	−10.74	Heated
HDP3	rNo. 9	7.18	1.971	−10.28	1.970	−10.28	Heated
HDP3	rNo. 10	4.26	1.450	−10.71	1.451	−10.71	Heated
HDP3	rNo. 11	4.75	1.558	−10.61	1.564	−10.62	Heated
HDP3	rNo. 12	5.10	1.630	−10.56	1.631	−10.56	Heated
HDP3	rNo. 13	5.56	1.715	−10.47	1.726	−10.48	Heated
HDP3	rNo. 14	6.32	1.843	−10.42	1.826	−10.40	Heated
HDP3	rNo. 15	4.88	1.585	−10.65	1.561	−10.62	Heated
HDP3	rNo. 16	14.42	2.669	−9.75	2.641	−9.72	Not-heated
HDP3	rNo. 17	4.70	1.548	−10.63	1.548	−10.63	Heated
HDP3	rNo. 18	5.18	1.645	−10.55	1.645	−10.55	Heated
HDP3	rNo. 19	4.90	1.590	−10.60	1.588	−10.60	Heated
HDP3	rNo. 20	5.27	1.662	−10.54	1.660	−10.54	Heated
HDP3	rNo. 21	5.90	1.774	−10.42	1.785	−10.43	Heated
HDP3	rNo. 22	9.46	2.247	−10.09	2.227	−10.07	Not-heated
HDP3	rNo. 23	4.11	1.414	−10.77	1.401	−10.75	Heated
HDP3	rNo. 24	3.23	1.172	−10.99	1.149	−10.96	Heated
HDP3	rNo. 25	5.58	1.720	−10.48	1.724	−10.48	Heated

rNo. random number for unnumbered pieces. Roughness Ra and entropy *S* values on the left are measured on archaeological test samples; Ln(Ra) values are calculated from the measured data. Values under '*x* on function [Ln(Ra)]' are perpendicular projections of Ln(Ra) onto the function derived by fitting experimental reference measurements (for DFT2 samples) and internal reference measurements obtained from known archaeological pre- and post-HT scars (for HDP samples). Values under '*y* on function [S]' are the corresponding *y* coordinates on the fitted functions. Entries under 'Result' are obtained from the position of the projected values (their 1D variance) with respect to the overlap zone's position on these fitted functions. Thresholds are defined by the overlap zone in reference scatter plots and are [in Ln(Ra)] for DFT2 samples (obtained on the experimental reference): heated <2.12, indet. >2.12 < 2.65, not-heated >2.65a and for HDP samples (obtained from archaeological HDP pre- and post-HT scars): heated <2.123, indet. >2.123 < 2.157, not-heated > 2.157.

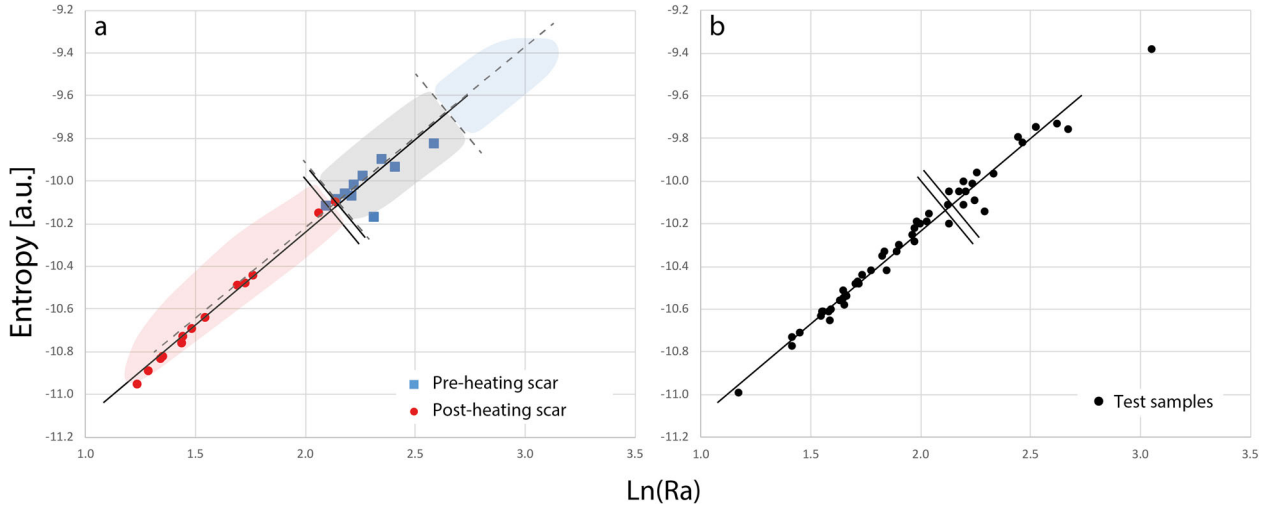

Fig. 3 Plots of the entropy S and mean roughness Ra values of archaeological samples from Hodjiespunt. a Plot of 23 known pre- (10) and post-heating (13) surfaces on diagnostic artefacts and their linear best fit (solid lines). The two solid black parallel lines mark the overlap zone in which both pre- and post-heating scars plot. Broken lines and coloured field are taken from the West Coast reference data in Fig. 2a. The lower and upper boundaries of the overlap zone [in Ln(Ra) at the intersection of the fitted function] are 2.12 and 2.16 for the solid lines. Note that both pre- and post-heating surfaces can be distinguished at the two extremities of the scatter plot. **b** Plot of 52 archaeological test samples onto the reference function and Indet.-zone of **a**.

were knapped after heat treatment. The observation of close to 70% heat-treated artefacts is in good agreement with most other MSA sites on South Africa's west and south coast. Similar data are known from the SB at Hollow Rockshelter (66–74%: Schmidt and Högberg, 2018), the HP at Diekploof (90–96%: Schmidt, 2019; Schmidt et al., 2015), Klipdrift (92%: Delagnes et al., 2016) and Mertenhof Shelter (37–78%: Schmidt and Mackay, 2016), the post-HP at Mertenhof (85–89%: Schmidt and Mackay, 2016) and even from the Later Stone Age at Elands Bay Cave (92%: Porraz et al., 2016). Thus, by ~130 ka, heat treatment was already fully mastered with no significant change occurring after that in terms of its prevalence. Two potential sources of error should, however, be taken into account: the precision of our estimation of heated artefacts and the dating of our HDP assemblage. Concerning the first source of error, measurement precision, we note that the number of heat-treated artefacts estimated visually and by roughness analysis is in good agreement. The major disagreement resides in the number of unheated artefacts. It was 8% higher when identified by surface roughness analysis than for visual inspection. The reason for this may be that visually some of the unheated artefacts were classified as indeterminate, while surface analysis allowed us to assign them to the Not-heated group. Scattering of data points around the fitted function is slightly better than for the DFT2 data with 0.0294, being similar to the mean distance obtained from our west coast reference collection data. Thus, measurement precision appears to be sufficient for comparing our HDP assemblage with more recent MSA ones. The second source of uncertainty is the dating of the analysed HDP assemblage. Only HDP1 was physically dated (Will et al., 2013), and we tentatively extended this date to HDP3 for our analysis, based on stratigraphy (following Parkington, 2003). While this is, in our opinion, likely to be correct, it might be wrong. If so, the relative prevalence of heat-treated silcrete artefacts securely attributed to 130–119 ka (those from HDP1) would be 65.7% (this percentage would be statistically less solid because it is calculated from 35 determinable pieces only). The relative prevalence of heat-treated silcrete artefacts from HDP3 would be 75.7% (as determined from 75 determinable pieces). Thus, our conclusion that close to 70% of all silcrete from between 130 and 120 ka at HDP was heat-treated still holds, even if we have wrongly assumed the age of our HDP3 assemblage.

Conclusion

What are the implications of our results for understanding the antiquity of silcrete heat treatment in southern Africa? The invention of heat treatment must predate 130 ka but postdate the DFT2 assemblage (dating somewhere between 400–200 ka). This is the time that *Homo sapiens* began to play a major role in the subcontinent (Dusseldorp et al., 2013) and it is the time that silcrete use appeared in the Cape coastal region (Will and Mackay, 2017). Early modern humans must have either transferred the idea from another similar technique or spontaneously invented heat treatment when they began using silcrete in the Cape region. A supplementary argument in the quest to identify the antiquity of heat treatment comes from Pinnacle Point, where Brown et al. (2009) suggested that silcrete might have been heat-treated as early as 164 ka. Unfortunately, the assemblage they published only contained 22 silcrete artefacts, 6 of which were reported to show stronger surface gloss than unheated reference samples. No photos of these pieces were shown in the publication and no information on the most unambiguous heating proxy, roughness contrast, was given. The data provided by Brown et al. (2009) are therefore insufficient to pronounce on whether the 165 ka Pinnacle Point assemblage documents an early stage of heat treatment. As it stands, the most likely scenario is that the invention of heat treatment occurred somewhere in the Cape coastal zone (where silcrete can be naturally found) between the appearance of *H. sapiens* in the region and 130 ka. Only future discoveries of new silcrete assemblages from before 130 ka will allow us to narrow down this gap of uncertainty.

What do our observations imply in terms of the reasons for inventing heat treatment? After 130 ka (and perhaps even in the one assemblage predating 130 ka), silcrete use seems to correlate with frequent heat treatment. However, it has been shown that silcrete can be, and sometimes was, also knapped without heat treatment (Schmidt and Mackay, 2016). It can therefore not easily be argued that early MSA knappers absolutely needed

the improvement in knapping quality to be able to use silcrete. Instead, the heat-fracturing hypothesis (Porraz et al., 2016; Schmidt et al., 2015) provides an interesting alternative explanation of why heat treatment might have been invented. Most types of rock react to rapid heating in fires by fracturing. Silica rocks like silcrete present the additional advantage of also improving in knapping quality. If early *Homo sapiens* regularly heat-fractured all types of stone raw materials before knapping, then they would also have done so with silcrete when they first encountered it. In such an operational scheme, early knappers can be expected to rapidly discover that silcrete is also knapped more easily when heat-fractured. At least the earliest improvements in knapping quality would in this case be no more than an unexpected by-product. This theory has important implications for understanding heat treatment as a proxy for archaeological and anthropological concepts like modernity or planning depth. Its test conditions are clear: it would become likely if raw materials other than silcrete from between ~300 and 130 ka would show signs of systematic heat-induced non-conchoidal fracturing after which knapping was continued. Examples of such rocks, commonly used to make tools in the southern African subcontinent, that do not improve in knapping quality but can potentially be heat-fractured are quartzite, dolerite and other igneous rocks. Investigating these test conditions, on the other hand, should prove to be more difficult, or at least labour intensive, as it is not easy to recognise heat-induced fracture surfaces on these types of stone raw materials without extensive experimental work. The stigmata produced on quartzite and different igneous rocks by heat-fracturing must first be analysed in terms of the mechanics that cause fracturing, then in terms of their roughness and surface structure, so that they can eventually be identified on artefacts.

Data availability

The data set generated for this study is available in Tables 1 and 2.

Received: 20 December 2019; Accepted: 31 March 2020;
Published online: 29 April 2020

References

Avery G, Halkett D, Orton J, Steele T, Tusenius M, Klein R (2009) The Ysterfontein 1 middle stone age rock shelter and the evolution of coastal foraging. South Afr Archaeological Bull 10:66–89

Binder D (1984) Systèmes de débitage laminaire par pression: exemples chasséens provençaux. In: Tixier J, Inizan ML, Roche H (eds) Préhistoire de la pierre taillée, 2: économie du débitage laminaire: technologie et expérimentation: IIIe table ronde de technologie lithique. Meudin-Bellevue, octobre 1982. Cercle de Recherches et d'Etudes Préhistoriques, Paris, pp. 71–84

Binder D, Gassin B (1988) Le débitage laminaire chasséen après chauffe: technologie et traces d'utilisation. In: Beyries S (ed) Industries lithiques, tracéologie et technologie. British Archaeological Reports, Oxford, pp. 93–125. vol International Series 411

Bordes F (1969) Traitement thermique du silex au Solutréen. Bull de la Société préhistorique française 66(7):197

Brown K, Marean C (2010) Wood fuel availability for heat treatment drives the rise and fall of silcrete as a raw material in the middle stone age of South Africa, "Abstracts of the PaleoAnthropology Society 2010 Meetings.". PaleoAnthropology 2010:A0001 –A0040

Brown KS, Marean CW, Herries AIR, Jacobs Z, Tribolo C, Braun D, Roberts DL, Meyer MC, Bernatchez J (2009) Fire as an engineering tool of early modern humans. Science 325(5942):859–862

Delagnes A, Schmidt P, Douze K, Wurz S, Bellot-Gurlet L, Conard NJ, Nickel KG, van Niekerk KL, Henshilwood CS (2016) Early evidence for the extensive heat treatment of silcrete in the howiesons poort at klipdrift shelter (Layer PBD, 65 ka), South Africa. PLoS ONE 11(10):e0163874. https://doi.org/10.1371/journal.pone.0163874

Dusseldorp G, Lombard M, Wurz S (2013) Pleistocene homo and the updated stone age sequence of South Africa. South Afr J Sci 109(5/6):1–6. https://doi.org/10.1590/sajs.2013/20120042

Goldberg P, Miller CE, Schiegl S, Ligouis B, Berna F, Conard NJ, Wadley L (2009) Bedding, hearths, and site maintenance in the Middle Stone Age of Sibudu Cave, KwaZulu-Natal, South Africa. Archaeol Anthropol Sci 1(2):95–122. https://doi.org/10.1007/s12520-009-0008-1

Hare, V (2020) Spoken personal communication (2020) reproduced here upon agreement of V. Hare

Inizan ML, Roche H, Tixier J (1976) Avantages d'un traitement thermique pour la taille des roches siliceuses. Quaternaria Roma 19:1–18

Inizan ML, Tixier J (2001) L'émergence des arts du feu: le traitement thermique des roches siliceuses. Paléorient 26(2):23–36

Klein RG, Avery G, Cruz-Uribe K, Halkett D, Hart T, Milo RG, Volman TP (1999) Duinefontein 2: an Acheulean site in the western cape province of South Africa. J Hum Evolution 37(2):153–190. https://doi.org/10.1006/jhev.1999.0307

Léa V (2004) Centres de production et diffusion des silex bédouliens au Chasséen. Gall préHist 46:231–250

Léa V (2005) Raw, pre-heated or ready to use: discovering specialist supply systems for flint industries in mid-Neolithic (Chassey culture) communities in southern France. Antiquity 79:1–15

Mandeville MD (1973) A consideration of the thermal pretreatment of chert. Plains Anthropologist 18:177–202

Marchand G (2001) Les traditions techniques du Mésolithique final dans le sud du Portugal: les industries lithiques des amas coquilliers de Várzea da Mó et de Cabeço do Rebolador (fouilles M. Heleno). Rev Portuguesa de Arqueologia 4 (2):47–110

Mourre V, Villa P, Henshilwood CS (2010) Early use of pressure flaking on lithic artifacts at Blombos Cave, South Africa. Science 330(6004):659–662

Parkington J (2003) Middens and moderns: shellfishing and the Middle Stone Age of the Western Cape, South Africa. South Afr J Sci 99:243–247

Patterson DB, Lehmann SB, Matthews T, Levin NE, Stynder D, Bishop LC, Braun DR (2016) Stable isotope ecology of Cape dune mole-rats (Bathyergus suillus) from Elandsfontein, South Africa: Implications for C4 vegetation and hominin paleobiology in the Cape Floral Region. Palaeogeogr, Palaeoclimatol, Palaeoecol 457:409–421. https://doi.org/10.1016/j.palaeo.2016.04.044

Porraz G, Igreja M, Schmidt P, Parkington JE (2016) A shape to the microlithic Robberg from Elands Bay Cave (South Africa). South Afr Humanities 29:203–247

Schmidt P (2014) What causes failure (overheating) during lithic heat treatment? Archaeol. Anthropol Sci 6(2):107–112

Schmidt P (2019) How reliable is the visual identification of heat treatment on silcrete? A quantitative verification with a new method. Archaeol Anthropol Sci 11(2):713–726. https://doi.org/10.1007/s12520-017-0566-6

Schmidt P, Buck G, Berthold C, Lauer C, Nickel K (2019) The mechanical properties of heat-treated rocks: a comparison between chert and silcrete. Archaeol Anthropol Sci 11(6):2489–2506

Schmidt P, February E, Bretzke K, Bellot-Gurlet L (2016a) Tempering-residue on heat-treated silcrete: an experimental perspective and a potential analytical protocol. J Archaeological Sci: Rep. 15:611–619

Schmidt P, Hiscock P (2019) Evolution of silcrete heat treatment in Australia-a regional pattern on the South-East Coast and its evolution over the Last 25 ka. J Paleolithic Archaeol 2:74–97

Schmidt P, Högberg A (2018) Heat treatment in the still Bay-A case study on Hollow Rock Shelter, South Africa. J Archaeological Sci: Rep. 21:712–720

Schmidt P, Lauer C, Buck G, Miller CE, Nickel KG (2017) Detailed near-infrared study of the 'water'-related transformations in silcrete upon heat treatment. Phys Chem Miner 44(1):21–31. https://doi.org/10.1007/s00269-016-0833-6

Schmidt P, Mackay A (2016) Why was silcrete heat-treated in the Middle Stone Age? An early transformative technology in the context of raw material use at Mertenhof Rock Shelter, South Africa. PLoS ONE 11(2):e0149243. https://doi.org/10.1371/journal.pone.0149243

Schmidt P, Paris C, Bellot-Gurlet L (2016b) The investment in time needed for heat treatment of flint and chert. Archaeol Anthropol Sci 8(4):839–848

Schmidt P, Porraz G, Bellot-Gurlet L, February E, Ligouis B, Paris C, Texier JP, Parkington JE, Miller CE, Nickel KG, Conard NJ (2015) A previously undescribed organic residue sheds light on heat treatment in the Middle Stone Age. J Hum Evolution 85:22–34

Schmidt P, Slodczyk A, Léa V, Davidson A, Puaud S, Sciau P (2013) A comparative study of the thermal behaviour of length-fast chalcedony, length-slow chalcedony (quartzine) and moganite. Phys Chem Miner 40(4):331–340

Sealy J (2009) Modern behaviour in ancient South Africans: evidence for the heat treatment of stones in the Middle Stone Age. South Afr J Sci 105:323–324

Shannon CE (1948) A mathematical theory of communication. Bell Syst Tech J 27 (4):623–656

Stolarczyk RE, Schmidt P (2018) Is early silcrete heat treatment a new behavioural proxy in the Middle Stone Age? PLoS ONE 13(10):e0204705

Terradas X, Gibaja JF (2001) El tratamiento termico en la produccion litica: el ejemplo del Neoltico Medio Catalan. Cypsela 13:31–58
Tiffagom M (1998) Témoignages d'un traitement thermique des feuilles de laurier dans le Solutréen supérieur de la grotte du Parpalló (Gandia, Espagne). Paléo 10:147–161
Wadley L (2013) Recognizing complex cognition through innovative technology in Stone Age and Palaeolithic Sites. Cambridge Archaeological. Journal 23 (02):163–183
Wadley L, Prinsloo LC (2014) Experimental heat treatment of silcrete implies analogical reasoning in the Middle Stone Age. J Hum Evolution 70(0):49–60
Wilke PJ, Flenniken J, Ozbun TL (1991) Clovis technology at the Anzick Site, Montana. J Calif Gt Basin Anthropol 13(2):242–272
Will M, Mackay A (2017) What factors govern the procurement and use of silcrete during the Stone Age of South Africa? J Archaeological Sci: Rep 15:630–645. https://doi.org/10.1016/j.jasrep.2016.11.046
Will M, Parkington JE, Kandel AW, Conard NJ (2013) Coastal adaptations and the Middle Stone Age lithic assemblages from Hoedjiespunt 1 in the Western Cape, South Africa. J Hum Evolution 64(6):518–537. https://doi.org/10.1016/j.jhevol.2013.02.012

Acknowledgements

Financial support for this study was provided by the Deutsche Forschungsgemeinschaft (DFG) (grant number SCHM 3275/2-1).

Competing interests

The authors declare no competing interests.

Additional information

Correspondence and requests for materials should be addressed to P.S.

Reprints and permission information is available at http://www.nature.com/reprints

Publisher's note Springer Nature remains neutral with regard to jurisdictional claims in published maps and institutional affiliations.